Eur. Phys. J. B **19**, 241–247 (2001)

THE EUROPEAN PHYSICAL JOURNAL B

EDP Sciences

Single-crystal like NMR spectra of $CeCu_5Au$ powder samples

E. Kerscher, M.T. Kelemen, K.H. Diefenbach, O. Stockert[a], H.v. Löhneysen, and E. Dormann[b]

Physikalisches Institut, Universität Karlsruhe (TH), Engesserstr.7, 76128 Karlsruhe, Germany

Received 19 June 2000

Abstract. Single-crystal like nuclear magnetic resonance spin-echo spectra are obtained for powder samples of the antiferromagnet $CeCu_5Au$ in the paramagnetic phase. Line shifts and quadrupolar splittings are analyzed for ^{63}Cu and ^{65}Cu. The influence of the extreme magnetic anisotropy of the $CeCu_{6-x}Au_x$ compounds on nuclear spin relaxation is discussed.

PACS. 76.60.-k Nuclear magnetic resonance and relaxation – 75.20.Hr Local moment in compounds and alloys; Kondo effect, valence fluctuations, heavy fermions

1 Introduction

The pseudo-binary intermetallic compounds $CeCu_{6-x}Au_x$ and the ternary compound $CeCu_5Au$ received considerable interest in recent years [1]. $CeCu_6$ is one of the best-known heavy-fermion systems with no magnetic order above 20 mK [2,3], the structurally ordered ternary compound $CeCu_5Au$ orders antiferromagnetically at $T_N = 2.3$ K [4] and for pseudobinary compounds $CeCu_{6-x}Au_x$ with $x \approx 0.1$ at the magnetic-nonmagnetic boundary for $T_N \to 0$ signatures of non-Fermi liquid behavior were found [5]. The reasonably simple orthorhombic room-temperature crystallographic structure (Pnma [6], see Fig. 1) favours more detailed analyses of the magnetic characteristics. The crystal field splitting (coefficients B_2^0, B_2^2, B_4^0, B_4^2, and B_4^4) of the Ce^{3+} six fold degenerate $^2F_{5/2}$ Hund's rule groundstate into three doublets $|0,\pm\rangle, |1,\pm\rangle$ and $|2,\pm\rangle$ with $|1\rangle$ and $|2\rangle$ lying about $\Delta_1/k_B \approx 100$ K and $\Delta_2/k_B \approx 160$ K above the ground state [7] gives rise to a pronounced low-temperature magnetic anisotropy (see also Fig. 2). Due to the predominance of the coefficient a_0 of the spin-orbit coupled crystal-field adapted wave function,

$$|n,\pm\rangle = a_n|\pm 5/2\rangle + b_n|\pm 1/2\rangle + c_n|\mp 3/2\rangle \qquad (1)$$

for the ground state $|0,\pm\rangle$, *i.e.* $|a_0|^2 \approx 90\%$ [7] an almost Ising-like magnetic anisotropy with c (orthorhombic description) as the preferred direction was reported already in early reports [8], see also Figure 2 for our current sample. Thus the magnetic anisotropy is one of the primary ingredients in the anomalous behavior of the compounds $CeCu_{6-x}Au_x$. In order to shed additional light on these peculiarities we report a nuclear magnetic resonance (NMR) analysis for a powder sample of $CeCu_5Au$ in its high-temperature paramagnetic phase in the following. We prove that single-crystal like NMR spectra can

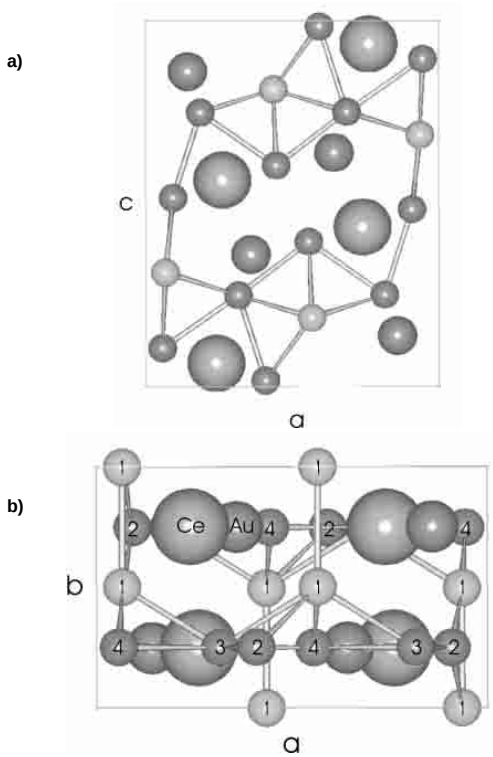

Fig. 1. Crystal structure of $CeCu_5Au$ [6] (sphere diameter increasing as Cu..Au..Ce), seen along b-direction (a), and against c-direction (b). In (b), two Cu(3) sites are hidden by Ce and Au atoms.

[a] *Present address:* H.H. Wills Laboratory, University of Bristol, Bristol, UK.

[b] e-mail: `edo@piobelix.physik.uni-karlsruhe.de`

Table 1. NMR data used in current analysis [13–15].

Isotope	^{63}Cu	^{65}Cu
abundancy	69.1%	30.9%
I	3/2	3/2
$\gamma/2\pi$/MHz/T	11.285	12.090
$Q/10^{-24}$ cm^2	−0.211	−0.195

be obtained for ^{63}Cu and ^{65}Cu (NMR data see Tab. 1) nevertheless, as was otherwise only accessible by zero-field nuclear quadrupole resonance (NQR) [9–12]. Magnetic and quadrupolar contributions are separated and the relevance of these results for the understanding of NMR properties in the parent $CeCu_6$ compound is stressed.

2 Experimental details

Single crystals of $CeCu_5Au$ were grown by the Czochralski method as described earlier [4–7]. The magnetic susceptibility was determined with a Quantum Design MPMS SQUID magnetometer and is shown in Figure 2 (measured at the field strength of NMR use). The sample contained about 2.5 μg Fe per g. For NMR measurements the crystal was appropriately cleaned, powdered under nitrogen atmosphere (20–50 μm grain size) and sealed in a quartz glass (Suprasil) ampoule. Two different samples A and B of $CeCu_5Au$ were used (ca. 600 mg).

The NMR data were recorded with a Bruker CXP 200 spectrometer, using the variable field of an electromagnet (< 1.9 T) or the fixed field (4.7 T) of a superconducting magnet. Variable temperature cryostats (Oxford instruments) were equipped with home-built probeheads with silver coils and copper-less sample space. 90°– and 180° – pulses of 2 μs and 4 μs were realized for the ^{63}Cu and ^{65}Cu isotopes. NMR spectra were recorded by the spin-echo technique for pulse separations of 50 μs or 75 μs. The second half of the spin-echo was Fourier transformed. The integral over the frequency range corresponding to the step-width of the spectral recording was plotted as signal amplitude *versus* frequency or field as shown in Figure 3 for example. Full phase cycling was required to reduce ringing and magnetoacoustic contributions [16,17]. The spin-echo attenuation (transversal relaxation time T_2) was analyzed with the 90°-τ-90°-τ spin echo sequence, the spin-lattice relaxation time T_1 was derived from the decay of the stimulated echo observed at $T+\tau$ in the 90°-τ-90°-$(T-\tau)$-90°-τ sequence.

3 Discussion of the results

3.1 Magnetic susceptibility

Figure 2 shows the pronounced magnetic anisotropy of a $CeCu_5Au$ single crystal measured at $B_0 = 4.7$ T appropriate for the following fixed-field NMR analyses. As

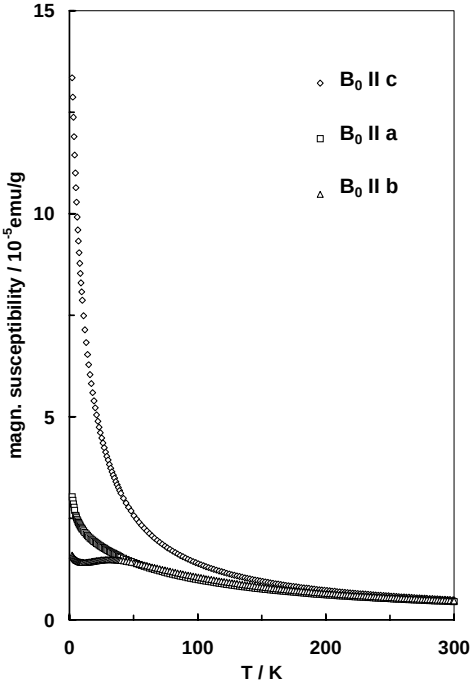

Fig. 2. Magnetic susceptibility of $CeCu_5Au$ single crystal for external magnetic field ($B_0 = 4.7$ T) along the crystallographic main axes.

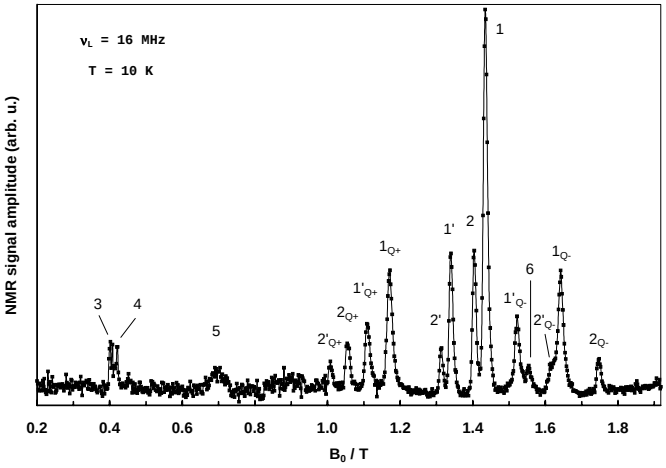

Fig. 3. $CeCu_5Au$-NMR spin-echo spectrum *versus* external magnetic field strength at 16 MHz NMR frequency ($T = 10$ K). The numbers are referred to in the text.

expected for the known level scheme, anisotropy is fully developed in the lowest temperature range only, whereas differences between a and b axis susceptibility are weak for temperatures above 50 K and high temperature isotropic average is approached at about 200 K. As can best be seen for B_0 parallel to the b axis, even the single crystal might contain a minor concentration of Ce^{3+} "impurity" sites reflected by the low temperature Curie tail. Powdering seems to increase this portion, as is most clearly visible from the Jaccarino-Clogston plots [13] presented in Figure 5. Finely powdered grains can be oriented at low

temperature and high field due to the strong magnetic anisotropy.

3.2 NMR "powder" spectra

In $CeCu_{6-x}Au_x$ with $0 < x \leq 1$, Au occupies the Cu(2) sites of the Pnma orthorhombic structure. There are four inequivalent Cu sites, which are numbered in Figure 1 ($a = 8.2455(4)$ Å, $b = 5.0866(3)$ Å, $c = 10.3659(5)$ Å in $CeCu_5Au$, [6]). Due to the low Cu site symmetry causing non-axial electric field gradients [16] and the existence of two isotopes differing in their NMR parameters (Tab. 1), highly complicated NMR powder spectra have to be expected in an external magnetic field. In this respect the $^{63}Cu/^{65}Cu$-NMR spectrum shown in Figure 3 as an example looks surprisingly simple and single-crystal like. NMR spectra were also recorded for fixed field of 4.7 T and variable frequency at various temperatures between 300 K and 4 K as well as at several other fixed frequencies between 14.2 MHz and 20 MHz as a function of magnetic field strength in order to distinguish different sites of the two isotopes, quadrupolar tensors and anisotropic hyperfine interaction. The main surprising conclusion is that the majority of the lines indexed in Figure 3 can be explained by one crystallographic surrounding and the assumption of the magnetic field being either parallel to the local (c-parallel) main axis of magnetic hyperfine and electrical quadrupolar interaction (lines 2, 2_{Q^+}, 2_{Q^-}) or along only one direction perpendicular to this main axis (lines 1, 1_{Q^+}, 1_{Q^-}), for both isotopes, *i.e.* ^{63}Cu and ^{65}Cu (the latters indicated as 1', 2',...).

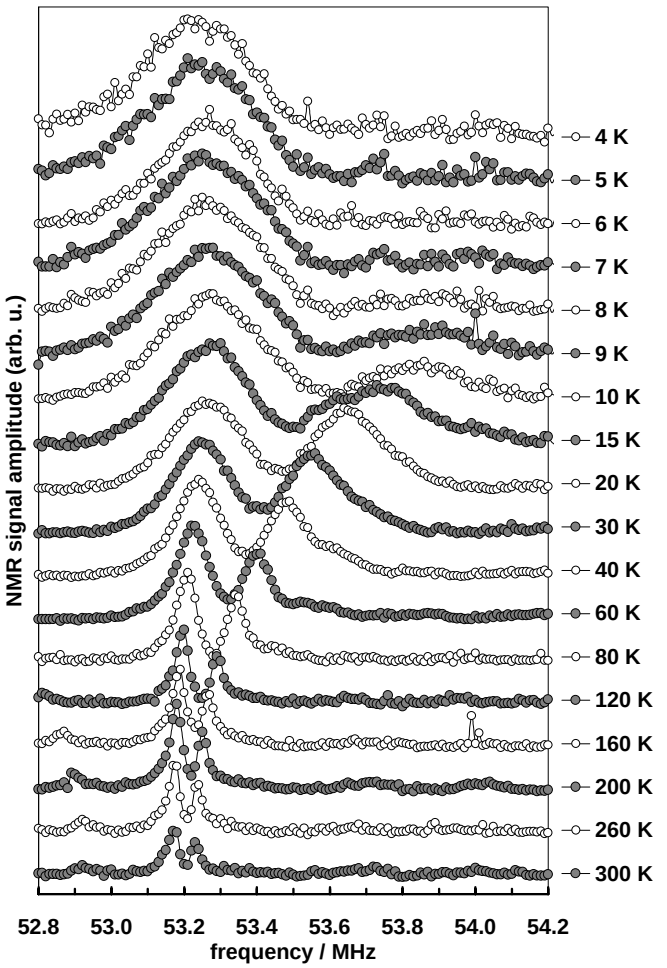

Fig. 4. Temperature dependence of central part of ^{63}Cu NMR spin-echo spectrum of $CeCu_5Au$ at $B_0 = 4.7$ T (lines 1 (lower frequency) and 2).

3.3 Central line analysis ("Zeeman-lines")

The primary key for the understanding of these powder spectra is the analysis of the temperature dependent shift and broadening of the central ^{63}Cu NMR lines ("Zeeman-lines" 1 and 2) shown in Figure 4. Both lines show severe broadening upon lowering of the temperature. Whereas the lower-frequency line exhibits only a minor line shift, the position of the high-frequency line varies drastically. It should be kept in mind that the spin-echo spectrum is plotted in Figure 4 for fixed pulse separation τ, *i.e.* not extrapolated to $\tau = 0$. Thus the relative intensities of both lines reflect also the difference of their T_2^{-1} echo decay rates, being rather similar for $T > 20$ K, but suppressing the shifted line 2 additionally for lower temperatures. For uniform intermetallic compounds and unique J, $S(4f) \leftrightarrow {}^{63,65}I$ transferred hyperfine coupling mechanism, we expect that the NMR line shift (temperature dependent Knight shift) varies as [13]

$$K(T) = \frac{\Delta\nu}{\nu_0} = K_0 + \alpha\frac{\chi_{\mathrm{mol}}(T)}{N_{\mathrm{A}}\mu_{\mathrm{B}}}, \qquad (2)$$

with the coupling constant α ranging between a few kOe/μ_{B} for transferred (classical) dipolar fields to several hundreds of kOe/μ_{B} for direct wavefunction overlap. The corresponding graphic solution of K *versus* χ with T as implicit parameter was termed historically "Jaccarino-Clogston plot" and is shown in Figure 5 for the two $CeCu_5Au$ powder samples "A" and "B" (with data for sample B being considered more reliably due to its more cautious sealing into its glass ampoule). Parts (a), (b) and (c) correlate the same line shift data of lines 1 and 2 alternatively with the three main axis susceptibilities χ_a, χ_b and χ_c. It is self-explanatory that the strongly shifted line 2 follows χ_c, thus originates from ^{63}Cu nuclei having their Ce^{3+} neighbours in an external magnetic field oriented along the magnetically preferred (Ising-like) c-axis (Fig. 5c). The corresponding coupling constant $\alpha_c = +1.59$ kOe/μ_{B} derived from the slope indicates that the contact interaction is not dominating dipolar contributions.

For line 1, the field orientation in the a-b plane is uncontroversal. The monotony of the data points of the more reliable sample B favours the association with the crystallographic a direction, which is the direction of intermediate strength of the low temperature magnetization. The corresponding coupling constant of $\alpha_\perp = +1.23$ kOe/μ_{B}

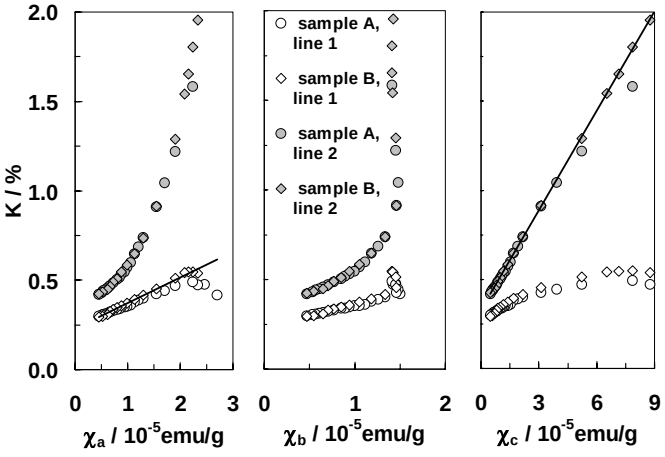

Fig. 5. Jaccarino-Clogston plots for ^{63}Cu NMR line shift of $CeCu_5Au$ powder sample. $K(T)$, derived from Figure 4, is plotted *versus* single-crystal total magnetic susceptibility (Fig. 2) with temperature as an implicit parameter, using the measured values of χ for the crystallographic main axes a (a), b (b) and c (c).

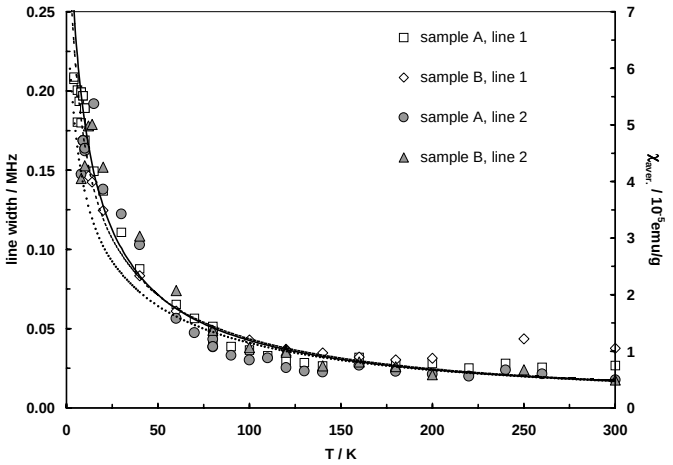

Fig. 6. Temperature dependence of ^{63}Cu NMR line width (lines 1 and 2) for $CeCu_5Au$ powder samples A and B (B_0 = 4.7 T). The lines show the scaled temperature dependence of the averaged magnetic susceptibility for the a-c plane (solid line), the b-c plane (dashed line) or all three orientations (dotted line).

is lower than α_c and might indicate an orientation resulting in partial compensation of classical dipolar contributions. Thus, both coupling constants are comparatively small, even for classical dipolar contribution [13]. It is evident, that the large difference in the size of the line shifts of lines 1 and 2 is mainly due to the anisotropy of the magnetic susceptibility, but amplified in addition by the anisotropy of the coupling constant. The positive sign of α should be considered, too. Generally, the transferred hyperfine field at the non-magnetic neighbours in rare earth intermetallic compounds is antiparallel to the electron spin moment orientation [13]. Due to the L minus S coupled configuration of the Hund's rule ground state of Ce^{3+}, the conduction electron transferred hyperfine field contribution will be parallel to the total electronic moment, as observed here. The anisotropy of α reflects thus the relative importance of the classical dipolar contribution, adding up for field orientation parallel to the c axis, but subtracting and reducing in magnitude for the perpendicular orientation.

The line broadening for lines 1 and 2 scales reasonably with the average magnetization for a-c or b-c plane, pointing to demagnetization broadening of both lines (Fig. 6). Thus the T-dependence of the lines 1 and 2 observed close to the bare gyromagnetic ratio of ^{63}Cu – and analogously lines 1' and 2' for ^{65}Cu – indicates that the NMR spectrum does not result from a powder distribution, but reflects only the behavior for the magnetic field parallel to the magnetically preferred c axis and one axis perpendicular to it, presumably the a axis.

3.4 Quadrupolar splitting

A detailed analysis of the line positions in all NMR spectra recorded for samples A and B *versus* field or frequency at various temperatures revealed that lines 2 and 2' are accompanied symmetrically by two quadrupolar satellites (indicated as 2_{Q^+} and 2_{Q^-} or $2'_{Q^+}$ and $2'_{Q^-}$, respectively, in Fig. 3). This is in agreement with a coincidence of the main axis of the electric field gradient (V_{zz}) and the c axis which is parallel to the external field for these lines. In contrast, the central lines 1 and 1' are shifted by a second order contribution with respect to their quadrupolar satellites, as is familiar for magnetic field perpendicular to the main axis of the electric field gradient. The various spectra were analyzed and fitted using the general expression [18]

$$\begin{aligned}\nu_{\mathrm{m,m-1}} = {} & \nu_0(\vartheta,\phi) \\ & + \frac{\nu_Q}{2}\left(\mathrm{m}-\frac{1}{2}\right)(3\cos^2\vartheta - 1 - \eta\sin^2\vartheta\cos(2\phi)) \\ & + \frac{\nu_Q^2}{32\nu_0}(1-\cos^2\vartheta)\Bigg[\left(102m(m-1)-\frac{57}{2}\right) \\ & \times \cos^2\vartheta\left(1+\frac{2}{3}\eta\cos(2\phi)\right) - \left(6m(m-1)-\frac{9}{2}\right) \\ & \times \left(1-\frac{2}{3}\eta\cos(2\phi)\right)\Bigg] + \frac{\eta^2}{72}\frac{\nu_Q^2}{\nu_0}\Big[24m(m-1)-6 \\ & - \left(30m(m-1)+\frac{9}{2}\right)\cos^2\vartheta \\ & - \left(\frac{51}{2}m(m-1)+\frac{21}{16}\right)\cos^2(2\phi)(\cos^2\vartheta-1)^2\Big].\end{aligned}$$

As shown in Figure 7, a rather convincing simulation of the spectra could be obtained with the quadrupole parameters compiled in Table 2. The simulation uses Gaussian lines for $\vartheta = 0$ (the V_{zz} and crystallographic c orientation) and $\vartheta = 90°$, $\varphi = 90°$ (the V_{yy} direction in the a-b plane, presumably parallel to the crystallographic a direction). For the third direction, only the central lines, coinciding then with the lines 1 and 1', can be accommodated in the spectra [17]. It is currently not clear whether

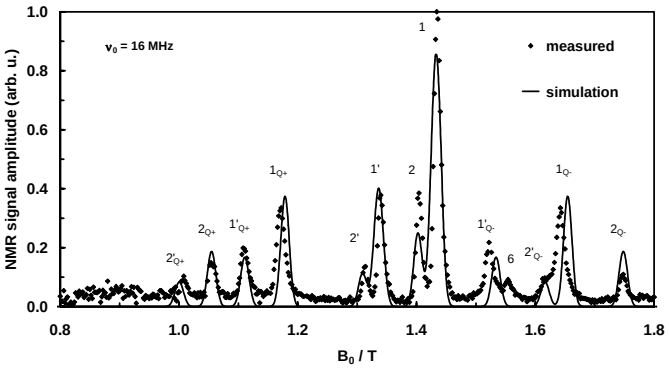

Fig. 7. Simulation of field dependent NMR spectrum of $CeCu_5Au$ at $\nu_0 = 16$ MHz. The respective quadrupole splitting parameters are compiled in Table 2. For further details see text.

Table 2. Quadrupole parameters derived *via* simulation of the $CeCu_5Au$ "powder" spectra ($T = 10$ K).

	$\nu_{Q,z}$	$\nu_{Q,y}$	η
^{63}Cu	3.90 MHz	2.65 MHz	0.36
^{65}Cu	3.64 MHz	2.48 MHz	0.36
ratio 63/65	1.07	1.07	

no grains are remaining in our powder samples with their *b*-axis (with weakest low-temperature susceptibility) oriented parallel to the external field (and thus B parallel to V_{xx}) or if the corresponding quadrupolar satellites are broadened to unvisibility due to variation of V_{xx} for the different crystallographic Cu sites. A much faster spin-echo decay of these lines could also explain that they remain unobserved in spin-echo spectra obtained with pulse separation of 50 μs to 75 μs. It should be emphasized that the ratio of the quadrupole parameters of both isotopes agrees within the error bar with that of their quadrupole moments (Tabs. 1 and 2). Lines 3 (^{65}Cu), 4 (^{63}Cu) and 5 (both isotopes), numbered in Figure 3 can be associated with normally "forbidden" transitions and only line 6, appearing in the quadrature-detected echo spectra with an unusual phase [17], is left unexplained and thus supposed to originate not from the sample studied here.

Thus in summary we showed that the powder spectra of our $CeCu_5Au$ samples resemble single-crystal NMR spectra with only one site and two mutually perpendicular field orientations. The corresponding main value of quadrupolar splitting ($\nu_{Q,z}$) falls close to the NQR frequency I (presumed site Cu(3)) reported for $CeCu_6$ [10,11]. It remains a puzzle why line shapes typical for powder distributions and the large number of inequivalent Cu sites are not observed.

3.5 Spin-echo decay (T_2) for central Cu NMR lines of $CeCu_5Au$

Due to the high concentration of ^{63}Cu and ^{65}Cu nuclear magnetic moments, it is no surprise that the spin echo decay in $CeCu_5Au$ can best be described by a Gaussian function $I(\tau) = A\exp(-4\tau^2/T_2^2)+B_{\rm noise}$ as usual for dominating nuclear dipolar interactions [19]. The corresponding decay constant T_2 is plotted in Figure 8.

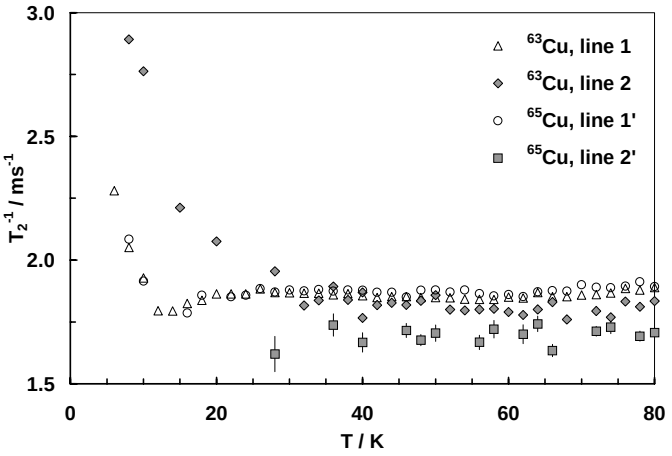

Fig. 8. Spin echo decay constant *versus* temperature for both Cu isotopes in $CeCu_5Au$ (central lines) at $B_0 = 4.7$ T, assuming Gaussian echo decay.

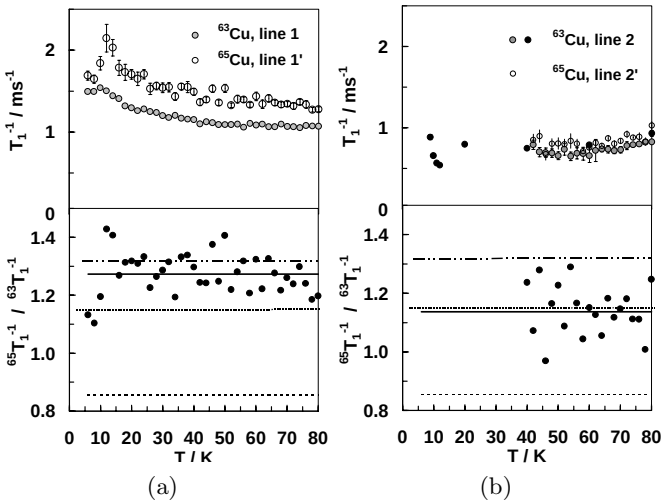

Fig. 9. Comparison of the temperature dependence of the spin-lattice relaxation rates for the two isotopes ^{65}Cu and ^{63}Cu. In the lower part, the observed ratio and its average value (solid line) is compared with $(^{65}Q/^{63}Q)^2$ (broken line), $(^{65}\gamma/^{63}\gamma)^2$ (dotted) and $(^{65}\gamma/^{63}\gamma)^4$ (dashed-dotted). (a) Lines 1, 1' for field in *a*-*b* plane. (b) Lines 2, 2' for field along *c*. Due to large temperature dependent shift, broadening and weak intensity, the error margin is large in the low-T range.

The rates T_2^{-1} are temperature independent for T above 30 K. In this T range the rates for the lines 2 and 2' (*i.e.* field parallel to *c*) are smaller than those of the lines 1 and 1'. In contrast, for temperatures approaching the Néel temperature the slowing down of antiferromagnetic fluctuations results in a remarkable increase of the decay rate T_2^{-1}, which is most pronounced for the preferred magnetic direction (*c* axis, lines 2).

3.6 Spin lattice relaxation rates (T_1) for $CeCu_5Au$

Not unexpectedly for quadrupole-split NMR lines in metallic solids, it is difficult to derive reliable spin-lattice relaxation data for the powder sample studied here. Thus thin single-crystalline foils would present a better experimental starting point [13]. At about 80 K, the T_1^{-1} rates of all central lines (1, 2, 1', 2') are similar and of the order of 1 ms^{-1}. Figure 9a shows that T_1^{-1} increases by about 50% for the lines 1 and 1', if T is lowered to 6 K. The ratio of the rates for the two isotopes is constant and close to $(^{65}\gamma/^{63}\gamma)^4$, pointing to the relevance of direct or indirect nuclear magnetic dipole-dipole interactions for the relaxation path of the Cu sites with magnetic field in the a-b plane (a direction). Evidently, this behavior is far from a Korringa rate $T_1^{-1} \sim T$ due to the Fermi contact interaction with conduction electrons.

For the NMR lines 2, 2' corresponding to magnetic field parallel to the magnetically preferred c axis, the large line shift and broadening reduces the reliability of the relaxation data. Smaller T_1^{-1} rates are observed, with their ratio for both isotopes close to $(^{65}\gamma/^{63}\gamma)^2$ typical for hyperfine contributions (transferred fields from $4f$ moments or conduction electrons). This T_1^{-1} rate decreases with temperature at least for T above 50 K (also compatible with a Korringa-like contribution), but increases again for temperature approaching the magnetic ordering temperature.

These differences of spin-lattice relaxation behavior for varied orientation of the external field with respect to the crystallographic main axes testify that the relaxation mechanisms can reliably only be distinguished for oriented single crystals and exclusion of the influence of skin effect and magnetic impurities by appropriate sample preparation.

3.7 Comparison with $CeCu_6$

Low temperature spin-lattice relaxation rates of the "Zeeman lines" differing by more than a factor of three for varied field orientation in $CeCu_5Au$ point to difficulties to be expected in an analysis of the temperature dependent T_1^{-1} rates for the central $+1/2 \leftrightarrow -1/2$ nuclear spin NMR transition of, *e.g.*, ^{63}Cu in powder samples of the parent heavy fermion compound $CeCu_6$. Figure 10 shows that the temperature dependent spin-lattice relaxation rate can approximately be described by $T_1^{-1} = 0.5\ ms^{-1} + 0.0031\ ms^{-1} \times T/K$, if the decay of the stimulated echo amplitude is described by a single exponential function. This may be compared with the 3.5 times slower temperature independent spin-lattice relaxation rate for the 3.9 MHz NQR line of ^{63}Cu in $CeCu_6$ of $T_1^{-1} = 0.15\ ms^{-1}$ reported in [10] for T between the Kondo temperature $T_K = 6$ K and 30 K. If, instead, the stimulated echo decay is described by two exponential functions [16] the combination of a slow and a fast decay rate for the central ^{63}Cu NMR line improves the fit and gives the solid-symbol data in Figure 10. Evidently this analysis, suggested by the behavior of the "simple" antiferromagnetically ordering $CeCu_5Au$ compound, unravels low-temperature relaxation anomalies with much better resolution.

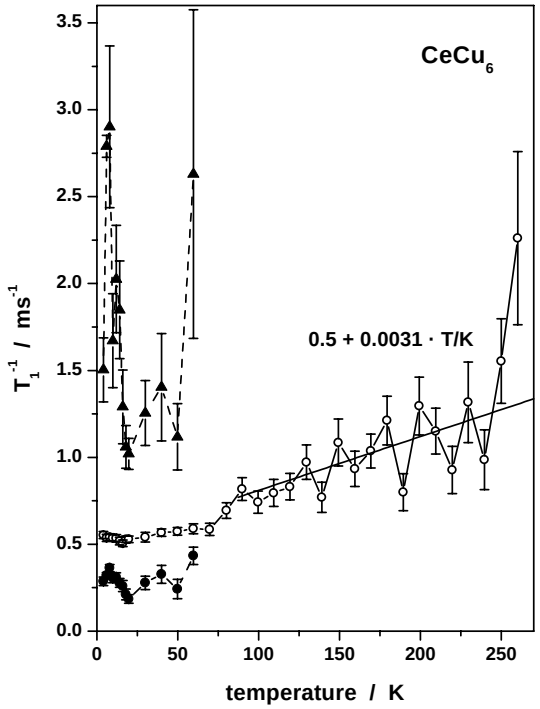

Fig. 10. Spin-lattice relaxation rate for ^{63}Cu in $CeCu_6$ at $\nu_0 = 53.2$ MHz, $B_0 = 4.7$ T (90° pulse of 1 μs). Description by one single (open circles) or two exponential functions (filled symbols).

4 Concluding remarks

We have shown that $CeCu_5Au$-powder NMR spin-echo spectra do not resemble powder spectra, but exhibit single-crystal characteristics, with contributions of only one Cu site and two field orientations and the familiar ratios of ^{63}Cu to ^{65}Cu gyromagnetic and quadrupolar parameters sufficient for the description of these spectra. The single-ion magnetic anisotropy of Ce^{3+} in its crystal field doublet ground state outweights all other influences: Due to the predominant $|\pm 5/2\rangle$ character of this doublet, the electronic magnetic susceptibility is very large only for magnetic field parallel to the c-direction, with a magnetization ratio of about $M_c : M_a : M_b = 8.4 : 1.9 : 1$ observed at the lowest temperature analysed here (*i.e.* $T = 2.5$ K, $B_0 = 4.7$ T). This general behaviour is reflected by the anisotropy of the paramagnetic (Knight) shift observed for the ^{63}Cu-NMR signal: In the range of a ΔK_c variation by 1.5%, $\Delta K_{\perp c}$ changes by 0.25% only. We have shown, however, that the relevant indirect hyperfine coupling constant α differs by about 23% only for these two directions, *i.e.* $\alpha_c = +1.59$ kOe/μ_B *versus* $\alpha_{\perp c} = +1.23$ kOe/μ_B. Thus the exchange integral between Cerium $4f$ spin and conduction electrons is not

unusually anisotropic in $CeCu_5Au$ – rather the crystal field clamps the spin-orbit-coupled moment to the c-axis, and allows at best a minor a-axis moment. An interesting question is how the single-ion anisotropy affects the recently found unusual scaling for the dynamical susceptibility at the quantum critical point for $x = 0.1$ [20].

We have further shown that the nuclear spin lattice relaxation mechanism of $^{63/65}Cu$ ($I = 3/2$) nuclei in $CeCu_5Au$ actually seems rather anisotropic: only for magnetic field parallel to the c-axis, does the hyperfine interaction, *i.e.* electron spin-nuclear spin coupling appear to predominate. For the orthogonal direction, nuclear spin-nuclear spin coupling (be it directly or indirectly mediated by conduction electrons or Cerium van Vleck-like contributions) seems to prevail. The weakness of powder NMR spectroscopy and data analysis needs to be emphasized, however. Only an even more detailed single-crystal foil NMR analysis may help unravelling the interplay between the extreme magnetic anisotropy, $4f$-electron-conduction electron and indirect $4f$-$4f$ exchange interactions as well as conduction-electron properties in the sequence paramagnetic heavy-fermion system – non-Fermi liquid – anisotropic heavy-fermion antiferromagnet in pseudobinary $CeCu_{6-x}Au_x$ intermetallic compounds.

We thank the Ministerium für Wissenschaft und Forschung Baden-Württemberg for early financial support of this project within the Forschungsschwerpunktprogramm Baden-Württemberg.

References

1. H.v. Löhneysen, J. Magn. Magn. Mater. **200**, 532 (1999).
2. Y. Onuki, T. Komatsubara, J. Magn. Magn. Mater. **63-64**, 281 (1987).
3. A. Amato, D. Jaccard, J. Flouquet, F. Lapierre, J. Tholence, R.A. Fisher, S.E. Lacy, J.A. Olsen, N.E. Phillips, J. Low Temp. Phys. **68**, 371 (1987).
4. C. Paschke, C. Speck, G. Portisch, H.v. Löhneysen, J. Low Temp. Phys. **97**, 229 (1994).
5. H.v. Löhneysen, T. Pietrus, G. Portisch, H.G. Schlager, A. Schröder, M. Sieck, T. Trappmann, Phys. Rev. Lett. **72**, 3262 (1994).
6. M. Ruck, G. Portisch, H.G. Schlager, M. Sieck, H.v. Löhneysen, Acta Cryst. B **49**, 936 (1993).
7. B. Stroka, A. Schröder, T. Trappmann, H.v. Löhneysen, M. Loewenhaupt, A. Severing, Z. Phys. B **90**, 155 (1993).
8. J. Rossat-Mignod, L.P. Regnault, J.L. Jacoud, C. Vetter, P. Lejay, J. Flouquet, E. Walker, D. Jaccard, A. Amato, J. Magn. Magn. Mater. **76-77**, 376 (1988).
9. T. Shimizu, M. Takigawa, H. Yasuoka, Y. Onuki, T. Komatsubara, J. Phys. Soc. Jpn **54**, 470 (1985).
10. Y. Kitaoka, K. Fujiwara, Y. Kohori, K. Asayama, Y. Onuki, T. Komatsubara, J. Phys. Soc. Jpn **54**, 3686 (1985).
11. K. Kumagi, I. Watanabe, H. Nakajima, Y. Onuki, T. Komatsubara, Jap. J. Appl. Phys. **26**, Suppl. 26-3 (1987).
12. T. Omuta, K. Fujiwara, T. Takeuchi, Y. Kohori, T. Kohara, Physica B **259-261**, 378 (1999).
13. E. Dormann, *NMR in intermetallic compounds*, in *Handbook on the physics and chemistry of rare earths*, edited by K.A. Geschneidner, L. Eyring, Vol. 14, Chap. 94 (Elsevier Science Publishers B.V., North-Holland, 1991).
14. Bruker, *Almanach* (Rheinstetten/Karlsruhe, 1999).
15. D.R. Lide, *CRC Handbook of Chemistry and Physics*, 76th edn. (CRC Press, Inc., Boca Raton, Florida, 1995-96).
16. K.H. Diefenbach, Diplomarbeit, Universität Karlsruhe (1998), unpublished.
17. E. Kerscher, Diplomarbeit, Universität Karlsruhe (2000), unpublished.
18. G.C. Carter, L.H. Bennett, D.J. Kahan, *Metal shifts in NMR*, in *Progress in Material Science*, Vol. 20, edited by B. Chalmers, J.W. Christian, T.B. Massalski (Pergamon Press, 1977).
19. A. Abragam, *The principles of nuclear magnetism* (Clarendon Press, Oxford, 1973).
20. A. Schröder, G. Aeppli, R. Coldea, M. Adams, O. Stockert, H.v. Löhneysen, E. Bucher, R. Ramazashivili, P. Coleman, Nature **407**, 351 (2000).